THE ASTROPHYSICAL JOURNAL, 283:24–32, 1984 August 1

THE EFFECT OF THE PERTURBATION OF THE LOCAL VELOCITY FIELD BY VIRGO ON THE CALCULATION OF DIFFERENTIAL LUMINOSITY FUNCTIONS

R. C. KRAAN-KORTEWEG
Astronomisches Institut der Universität Basel

ALLAN SANDAGE
Mount Wilson and Las Campanas Observatories of the Carnegie Institution of Washington

AND

G. A. TAMMANN[1]
Astronomisches Institut der Universität Basel; and European Southern Observatory, Garching
Received 1983 December 19; accepted 1984 January 13

ABSTRACT

We have repeated the determination of $\varphi(M)$ for galaxies in the *Revised Shapley-Ames Catalog* using Virgocentric perturbation fields of different strength to counter criticism that past calculations of the luminosity functions for galaxies of various Hubble types and van den Bergh luminosity classes are significantly in error as a result of neglect of this local velocity perturbation. Differential luminosity functions are given for 18 different Hubble types and luminosity classes for perturbation models with infall velocities of our Galaxy to Virgo of $v_{Vc} = 0$ (the null model for comparison), 220, and 440 km s^{-1}. The results, presented both by (v_H, M_B^0)-diagrams and by diagrams of the luminosity functions themselves show (1) that the change of shape of the upper envelope to the (v_H, M_B^0)-distributions is negligible compared with the null case, even for the extreme model with $v_{Vc} = 440$ km s^{-1}, and (2) the luminosity functions do not become significantly tighter in the perturbed models as the perturbation strengthens. The conclusion is that any realistic perturbation of the local velocity field does not introduce large enough errors in the calculation of $\varphi(M)$ to change the earlier result that a very large dispersion exists in M_B^0 within any given Hubble type and/or luminosity class.

Subject headings: galaxies: clustering — galaxies: photometry — galaxies: redshifts — luminosity function

I. INTRODUCTION

With the completion of the *Revised Shapely-Ames Catalog* (RSA, Sandage and Tammann 1981) with its known incompleteness as a function of apparent magnitude (Sandage, Tammann, and Yahil 1979, hereafter STY), it became possible to study the luminosity function of the RSA galaxies as a function of the van den Bergh luminosity class. The most unexpected result of the analysis (Tammann, Yahil, and Sandage 1979, hereafter TYS) was that the differential luminosity function $\varphi(M)$—even for galaxies within a narrow luminosity class—was quite broad, and that every luminosity class overlapped the luminosity functions of all other luminosity classes no matter how late the class (see Figs. 1, 3, and 4 of TYS). As a consequence of the large dispersion in M within each individual function, there is necessarily a strong correlation between the *mean* absolute magnitude of any subset of the RSA galaxies and their distances; the more distant galaxies have a brighter mean luminosity than the nearer ones in any sample taken from a catalog limited at its faint end by an apparent magnitude cutoff, as is the RSA at $B \approx 13.2$. The effect is, of course, the Malmquist bias. It is shown directly in plots of individual M_B-values versus redshift, such as Figures 1–4 of STY, and in Monte Carlo simulations made by Spaenhauer at Basel to specifically illustrate the effect in a pedagogical demonstration given elsewhere (Tammann and Sandage 1982).

The severity of the effect for the RSA galaxies has been somewhat questioned in two recent papers, one by Kennicutt (1982) and the other by de Vaucouleurs (1983). Kennicutt suggests that the broadness of the individual $\varphi(M)$ functions is not so great as in TYS if the calculation of $\varphi(M)$ takes into account the velocity perturbation on the ideal Hubble flow caused by the Virgo overdensity, an effect claimed by TYS to be small enough to be neglected. For the same reason as Kennicutt, de Vaucouleurs states that the variation of M_B with redshift given in Figures 1–4 of STY is smaller than shown, and therefore, that the Malmquist bias for the RSA galaxies within any given Hubble type and van den Bergh luminosity class is not so severe, justifying, in part, his compressed distance scale, based on his Λ-index.

The physics of the problem is that the perturbation causes an extra velocity component in addition to the general expansion value, sometimes adding, sometimes subtracting from the ideal Hubble flow, causing distances and hence absolute magnitudes calculated from the redshift alone to have a component of error. The size of the error depends on the size of the velocity perturbation, measured, for example, by the infall velocity of our Galaxy toward Virgo. Kennicutt calculated the distances of a subset of the RSA galaxies using a high infall velocity of 300 km s^{-1}. He claimed a major effect on the luminosity functions of spirals of different luminosity classes. De Vaucouleurs pointed out that the error in the M_B-values (calculated from the redshift) is correlated with the perturbations on the redshifts themselves in such a way as to affect the upper envelope of the STY diagrams in their Figures 1–4.

Because TYS believed that the effects of the velocity perturbations due to Virgo were so small, we doubted these separate results of Kennicutt and de Vaucouleurs, and have analyzed the problem anew using a new catalog of the velocity pertur-

[1] Visiting Associate, Mount Wilson and Las Campanas Observatories.

bations due to Virgo, calculated for each galaxy in the RSA for different adopted infall velocities by one of us (Kraan-Korteweg 1984). The results of this analysis are given in this paper. The problem is easiest to visualize from a study of the (M_B, log v)-diagram, and we discuss the effect of various velocity perturbations on the upper envelope of this plot in the next section. This leads into the discussion of the effect of these velocity perturbations on the individual luminosity functions in § III. Our conclusion is that even in the unrealistically severe case of an infall velocity of $v_{Vc} = 440$ km s^{-1}, the individual luminosity functions are still very broad, the Malmquist bias is essentially as severe as claimed by TYS, and de Vaucouleurs's Λ-index, upon which his distance scale beyond the Local Group is based, must necessarily have a large dispersion in absolute magnitude.

II. EFFECT OF THE VELOCITY PERTURBATION ON THE CALCULATION OF ABSOLUTE MAGNITUDES

a) Method of Calculation

The effect of the overdensity of the Virgo complex on the local velocity field is calculated here using the Virgocentric model first introduced by Silk (1974) and applied to data by Peebles (1976). The essence of the method is to consider mass shells concentric with the Virgo center that expand away from the center, each suffering a different deceleration due to the mass inside each particular shell. Because the density increases toward the cluster center, the shells closest to the center show the largest deceleration. Each shell is a miniature Friedmann universe whose motion is governed by the normal Friedmann $R(t)$ equation for the unfolding of the scale factor in time, but the nonuniform distribution of the matter requires each shell to be treated as its own universe. The time dependence of the motion of each shell can be followed, and the view of the instantaneous velocity field from any non-Virgocentric position of the perturbed velocity field can be reconstructed. Such a view from the position of our Galaxy at 22 Mpc from the cluster center is neatly summarized in a diagram first made by Tonry (1980). A version of the diagram for the very large infall velocity of 400 km s^{-1} is shown by Tonry and Davis (1981). A Tonry diagram for an infall of 220 km s^{-1}, calculated by U. Kaeser at Basel, has been shown by Sandage and Tammann (1983*a*). Comparison of these two diagrams shows the sensitivity of the velocity perturbation to the size of the infall velocity.

We model the problem by assuming an underlying noiseless Hubble expansion field upon which an idealized Virgocentric velocity perturbation is superposed. The perturbing excess mass at the Virgo Cluster is assumed to be spherically symmetric and to decrease with Virgocentric distance d as d^{-2}. Observational evidence for these assumptions is given in Yahil, Tammann, and Sandage (1980, hereafter YTS).

The total observed radial velocity of any given galaxy is its Hubble (cosmological) velocity v_H, plus the perturbed component v_g, plus any random radial velocity v_{noise} of the particular galaxy. The perturbation due to Virgo is the velocity vector pointed toward the Local Group of the Virgocentric infall velocity of any given galaxy. Clearly

$$v_{obs} = v_H + v_g + v_{noise} . \quad (1)$$

By v_{obs} we mean the velocity which an observer at the centroid of the Local Group would measure.

One can now write an exact solution for the idealized radial velocity in the noiseless case as

$$\begin{aligned} v_{model} &\equiv v_H + v_g \\ &= v_{Virgo} \frac{h_u x - (h_u - h_l)\cos\theta - (x - \cos\theta)[h_u - h_g(x)]}{h_l} \\ &= 1v_{Virgo}\left\{\cos\theta - \left[\frac{h_g(x)}{h_l}\right]\right\}(\cos\theta - x) . \end{aligned} \quad (2)$$

This is equation (6) of Schechter (1980) with the misprint in the denominator corrected. The definition of the h functions is also given there. A full explanation is in Kraan-Korteweg (1984).

The distance x of a galaxy is in units of the Virgo distance (i.e., $x \equiv r/r_{Virgo}$), θ is the angle between the galaxy and the Virgo Cluster center, and v_{Virgo} is the *observed* mean velocity of the Virgo Cluster reduced to the centroid of the Local Group. Equation (2) has been used to calculate x for every RSA galaxy (Kraan-Korteweg 1984) for various values of the Virgo density contrast.

Before discussing the normalization of equation (2) which is necessary to calculate x, it is useful to consider the linear approximation of equation (2) given by Schechter (1980):

$$v_{model} = v_{Virgo}x - v_{Vc}(\cos\theta - x) \times [1 - (x^2 - 2x\cos\theta + 1)^{-1}] , \quad (3)$$

where v_{Vc} is the infall velocity of our Galaxy toward Virgo. This is the approximation used by Kennicutt too derive his values. It is accurate enough for all regions not too close to the Virgo Cluster, so that any differences between our conclusions and his cannot be due to the different equations used to derive x.

The calculation of x from equation (2) or (3) is not quite straightforward. First, the transcendental equations cannot be solved directly for x. The solution is found by a nonlinear optimization method to be explained. Second, the term $v_{model} = v_H + v_g$ is not the observed velocity known to the astronomer, except in the absence of any random noise component. Hence, when v_{obs} from observational data is used in equation (2) in place of v_{model} to find x, any noise is propagated as an error in x. The effect is not severe for field galaxies if v_{noise} is smaller than $\sim$100 km s^{-1}, as we believe (Sandage and Tammann 1983*a*) but would be serious for the extremely large value of $\sim$350 km s^{-1} advocated by Davis and his collaborators (Davis, Geller, and Huchra 1978; Geller and Davis 1978). Discussion of why such a large random noise seems improbable is given elsewhere (Sandage and Tammann 1984).

The distances of any galaxy can be evaluated with equation (2) as soon as the nonlinear model for the Virgocentric flow is fixed. This is done by adopting three parameters: (*a*) the variation of the density excess with Virgocentric distance [$\rho(d) \propto d^{-2}$], (*b*) the density ratio of the sphere around the Virgo center with our Galaxy at its periphery to the background ($\rho_l/\rho_u = 3.8$ and 3.0 for $v_{Vc} = 220$ and 440 km s^{-1}, respectively), and (*c*) the mean observed velocity v_{Virgo} and our own infall velocity v_{Vc}, which essentially determines the Hubble parameter ratios $h_u/h_l = (v_{Vc} + v_{Virgo})/v_{Virgo} = 1.23$ and 1.46, respectively. With the known density run $\rho(d)$, the ratios ρ_l/ρ_u and h_u/h_l, the nonlinear flow model is defined.

Since every galaxy in this model has its own assigned mass shell with its corresponding miniature Friedmann universe, the Hubble parameter h_g and the density parameter Ω_g will differ for every galaxy. This is the reason why, in the nonlinear case,

the infall velocity v_g of any galaxy is not proportional to the density alone; hence a third parameter which is the background density ρ_u is necessary to define the model.

Relative distances x can now be calculated from equation (2) by a nonlinear optimization method. This is done in practice by determining $\rho_g(x)$, the average density in a sphere around Virgo with the considered galaxy at its periphery, and then $h_g(x)$, which is the corresponding Hubble parameter. As soon as the distance to the Virgo Cluster is specified, the x-values can be transformed into true distances by $r = xr_{\rm Virgo}$.

In passing, it is clear that the unperturbed (Hubble) velocity which would have been observed in the absence of any velocity perturbation is given by

$$v_{\rm H} = x(v_{\rm Virgo} + v_{\rm Vc}) = Hxr_{\rm Virgo} \qquad (4)$$

for any assumed value of the Hubble constant and Virgo distance.

The relative distances x and the actual distances r of the RSA galaxies used here have been from the catalog of these quantities previously mentioned (Kraan-Korteweg 1984), based on $v_{\rm Virgo} = 967$ km s^{-1} (Kraan-Korteweg 1981), $r_{\rm Virgo} = 21.7$ Mpc, corresponding to $(m - M)^0 = 31.67$, and three values of $v_{\rm Vc}$: 0, 220, and 440 km s^{-1}. These infall velocities almost certainly bracket the true situation. The best experimental data now favor $v_{\rm Vc} \approx 200$ km s^{-1} (Sandage and Tammann 1983*a*, 1983*b*, 1984; Dressler 1984). Values as high as 400 km s^{-1} are almost certainly excluded by the best current data. The adopted distance to Virgo is consistent with the value found in previous papers in the distance scale series (Sandage and Tammann 1982 [Paper VIII], and references therein). It is now supported by the expansion parallax of the supernova SN 1979c in NGC 4321 (Branch *et al.* 1981; Panagia *et al.* 1980) and also by an analysis of the infrared Tully-Fisher relation (Sandage and Tammann 1983*b*).

We stress that the main conclusion of this paper on the effect of $v_{\rm Vc}$ on the *shape* of $\varphi(M)$ depends only on the choice of the three observational parameters $\rho(d)$, ρ_u/ρ_l, $v_{\rm Vc}$, which define the infall model, *and is independent of the distance scale.* Only where we want to illustrate the results with realistic values of the absolute magnitudes and therefore linear distances does the choice of the absolute distance to Virgo, and hence the value of the Hubble constant, become necessary. However, once we choose the scale, a technical point is important in understanding the resulting absolute magnitudes in the three infall models. Once we adopt fixed parameters for the models we have no freedom as regards the global value of the Hubble constant. Its value is formally different for each of the infall models if we keep the distance to Virgo fixed. This is because the cosmological velocity of the Virgo Cluster [i.e., v(Hubble) in our previous notation] is different for the three infall models. Keeping the observed Virgo mean velocity to be 967 km s^{-1} gives the unperturbed Hubble cosmological velocity to be 967, 1187, and 1407 km s^{-1}, respectively, for infalls of 0, 220, and 440 km s^{-1}, which, with $r_{\rm Virgo} = 21.7$ Mpc, give the three values of H_0 to be 45, 55, and 65 km s^{-1} Mpc^{-1}, respectively, as the global value for the Hubble constant. Consequently, the absolute magnitudes for the same galaxy, calculated from

$$r = v_{\rm Virgo}(x/H_0) = v_{\rm H}/H_0 \ , \qquad (5)$$

will differ for the three infall models. This is essentially only a technical problem and does not mean that the actual zero point of the absolute magnitude system changes with the infall model. There is only one true value of the global Hubble constant, of the infall velocity, and of the cosmological recession velocity of the Virgo Cluster. We return to this point later when we compare the actual luminosity functions computed with the three assumptions concerning the infall velocity.

b) *The (v, M)-Diagram: Selection of the RSA Subsamples*

A useful diagram that shows at a glance the distribution of absolute magnitude at any distance is the plot of absolute luminosity as ordinate versus redshift (or distance) as abscissa. Such diagrams for radio galaxies and quasars using only the radio-bright sources of the 3CR Cambridge survey (Sandage 1972, Fig. 7) showed the extreme effect of the Malmquist bias there. The absolute luminosity of these very brightest of the radio sources in apparent flux appeared to increase in absolute luminosity as the square of the distance. The effect is due entirely to observational bias in the 3CR catalog, which cuts off at the very bright flux limit of 9 Jy, a situation analogous with the Shapley-Ames optical sample of galaxies.

The (v, M)-diagram is also particularly useful in calculating the luminosity function almost by inspection. Within each particular interval of $\Delta \log v$, the vertical distribution of points gives the $\varphi(M)$ function in the shell centered at the midpoint of the velocity interval. This $\varphi(M)$ can be connected with the $\varphi(M)$ in adjacent bins by a multiplicative factor that is merely the ratio of the volume elements. For a homogeneous distribution in space, the complete luminosity function can be built up by piecing together such segments, each normalized to the volume of its neighbor by multiplying by dex $3\Delta \log v_{\rm H}$. The procedure is strictly correct, of course, only if the galaxies are distributed uniformly in space so that the ratio of the numbers in adjacent shells of uniformly spaced $\Delta \log v$ is equal to the ratio of the volumes of the shells. But, in practice, even this assumption of a uniform distribution is not necessary if we merely assume that the shape of $\varphi(M)$ is the same from shell to shell, because we can shift each $\varphi(M)$ of a given shell onto that of any adjacent shell by an empirically determined vertical amount (which *would* be the ratio of the volumes in a homogeneous distribution) so as to give continuity in the resulting composite $\varphi(M)$. Because of our restriction of the final subsample of RSA galaxies to those away from the most serious place of the inhomogeneous distribution of galaxies near Virgo, as discussed below, we have, in fact, used only the simple volume scaling, neglecting any small inhomogeneity in the regions away from the Virgo complex. Justification for this point of procedure is given implicitly in the distribution maps discussed by YST.

Our first problem, i.e., the question of the stated objection of de Vaucouleurs (1983), reduces now to testing how much the (v, M)-diagrams differ from only another as the infall velocity is varied. We have divided the entire RSA sample into 18 subsamples, according to Hubble type and then to van den Bergh luminosity classes within each type, similar to the divisions made by TYS in their Tables 1 and 2. In the beginning, the justification for these binnings was that if, within any given Hubble type and vdB luminosity class, the absolute magnitudes had only a small dispersion, then this fact will be evident in the derived $\varphi(M)$ for that particular subset of galaxies. This was the initial result of van den Bergh (1960). It is also the stringent requirement that must be met by real galaxies if an index, Λ, formed by adding a number representing Hubble type to a number that codes vdB luminosity class (de Vaucouleurs 1979), is tightly correlated with absolute magnitude. Therefore, the present calculations can also be used to decide if the

TABLE 1

DIFFERENT BINS OF RSA GALAXIES CONSIDERED IN THIS PAPER

BIN			
Morph. Type	Lum. Class	N^a	$10\Lambda^b$
Sa, Sab	all	90	...
Sb	I–I.7	48	5
	I.8–II.2	20	6
	II.3–III.0	7	7.5
Sbc, Sc	I–I.7	91	7.5
	I.8–II.1	93	8.5
	II.2–II.7	63	9.5
	II.8–III.0	33	10.5
Sbc–Sm, Im	III.2–III.5	7	12.5
Sa–Sm, Im	I–I.7	151	8
	I.8–II.1	118	9
	II.2–II.7	68	10
	II.8–III.1	49	11
	III.2–III. 5	7	12
	I–III.5	393	...
E, E/S0	...	89	...
S0/E, S0, amorph.	...	99	...
E–S0, amorph.	...	188	...

[a] The number of galaxies in each bin.
[b] The approximate Λ-index of de Vaucouleurs.

Λ-index measures luminosity by testing the broadness of the $\varphi(M)$ functions at a given Λ-index. An earlier test that showed that within the Virgo Cluster itself Λ has a large dispersion (Tammann and Sandage 1982) is, then, now available using field galaxies as well.

The definition of the 18 subsamples is presented in Table 1. For two reasons the contents of individual bins, which are exactly the same as in TYS, will differ slightly. First, new type classification for 236 galaxies, prepared by Sandage (1982), were incorporated into the sample. Second, the area within a cone around the Virgo Cluster center, M87, with an opening angle of $\theta = 24\overset{\circ}{.}5$ was excluded. The reason for this exclusion can be visualized from the Tonry diagram in Tonry and Davis (1981): within this cone solutions for the distances x of equation (2) can be triple-valued for the infall model with $v_{Vc} = 440$ km s^{-1}. For this reason no galaxy within $\theta = 24\overset{\circ}{.}5$ from M87 was included in any of the three infall models. Of course, for $v_{Vc} = 220$ km s^{-1} the angle within which triple solutions are expected is smaller—$\theta = 16\overset{\circ}{.}5$ (cf. Sandage and Tammann 1983*a*), and for the null case of zero infall the velocities of galaxies within a radius of only 6° of M87 are no distance indicators. But to show best the changes in the (v, M)-diagrams and the changes in the luminosity functions which are due *solely* to the effect of the corrections for the Virgocentric motion, it is, of course, best to work with the same sample size for all three infall models; hence the same galaxies are excluded in all three cases.

Furthermore, to be consistent with TYS, RSA galaxies with $|b| < 30°$ were not included in the 18 bins because of the stronger discrimination of faint galaxies at low galactic latitudes and, moreover, because the completeness function of the RSA given in STY (which will be applied to the data later) is valid only for galaxies with $|b| \geq 30°$.

Together with the 18 bins themselves, Table 1 lists the total number of RSA galaxies that fulfill the conditions of $|b| \geq 30°$ and $\theta_{M87} > 24\overset{\circ}{.}5$, and an estimate of the de Vaucouleurs Λ-index, defined as $(L + T)/10$. The definitions of L and T are taken from the RC2 (de Vaucouleurs, de Vaucouleurs, and Corwin 1976).

c) *Differences in the (v, M)-Diagrams for the Three Infall Models*

To fix the ideas, we show in Figure 1*a* the (v_H, M_B^0)-diagram for the complete sample of E plus S0 galaxies for the null infall case to compare with the similar diagram in Figures 1, 2, and 3 of STY. Shown also is the upper envelope line from Figure 3 of that reference, and the lower cutoff due to the apparent magnitude limit of the Shapley-Ames at $m_B \approx 13.2$. The upper envelope line in Figure 1*a* here has been adjusted from the envelope line in Figure 3 of STY because the effective Hubble constant is required to be 45 with the present assumptions, compared with 50 in STY (see § II*b*). The adoption of this Hubble constant for zero infall results in a shift of 0.23 mag upward in luminosity and 0.05 to the left in log v_H. The envelope line is shown in both panels to assess the sensitivity of the plots to the infall effects.

Figure 1*b* is the (v_H, M_B^0)-diagram for the same galaxy types as in Figure 1*a*, but for the extreme infall velocity of 440 km s^{-1}. The abscissa in this panel is the cosmological velocity v_H (i.e., corrected for infall) calculated as $x\,(v_{Virgo}^{obs} + v_{Vc}) = v_{obs} + v_g$, with v_g as defined in equation (1). The envelope line is the

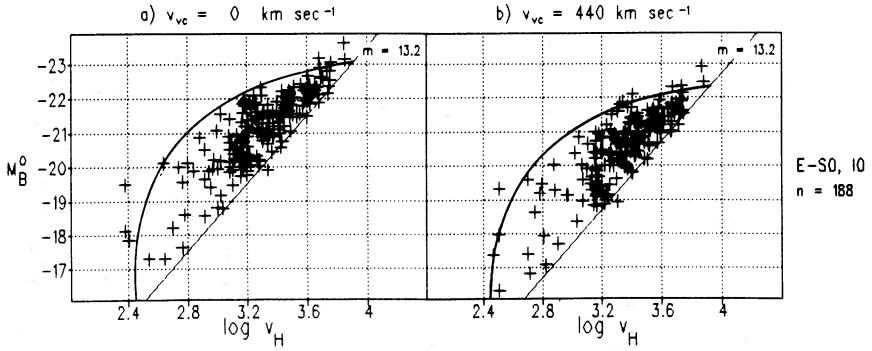

FIG. 1.—(*a*) The variation of the absolute magnitude M_B^0 with the ideal Hubble flow velocity v_H in the null perturbation model, i.e., where the infall velocity to Virgo is assumed to be zero. The sample is for Hubble types E and S0 from the RSA. Galaxies within $24\overset{\circ}{.}5$ radius of M87 are excluded. The upper envelope line computed by STY and adapted to the formal value of $H_0 = 45$ km s^{-1} Mpc^{-1} is shown. (*b*) Same as Fig. 1*a* for the infall model with $v_{Vc} = 440$ km s^{-1}. The upper envelope line is 0.8 mag fainter than in Fig. 1*a* because of the difference in the effective Hubble constant (see text).

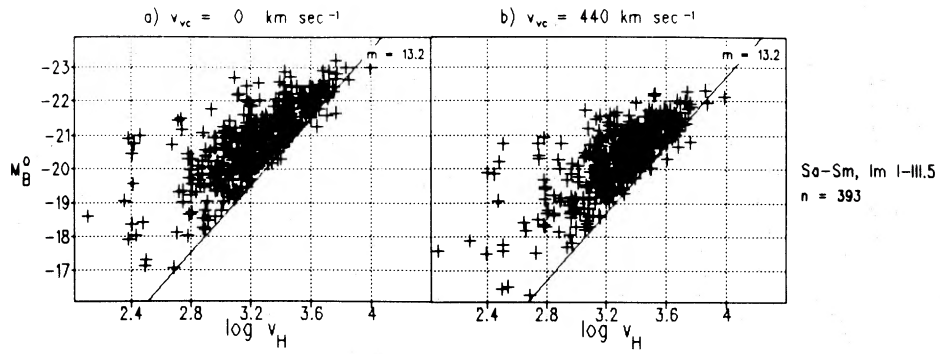

FIG. 2.—(*a*) Same as Fig. 1*a* for all spiral galaxies of luminosity classes I to III.5 for the zero infall model. The total number in the sample is 393. (*b*) Same as Fig. 2*a* for $v_{Vc} = 440$ km s^{-1}.

same as in Figure 1*a* but displaced upward by 0.8 mag to account for the technical difference in the Hubble constant; H_0 is 45 km s^{-1} Mpc^{-1} in Figure 1*a* and 65 km s^{-1} Mpc^{-1} in Figure 1*b*. It is clear that the distribution of points in both panels of Figure 1 and also the fit of the envelope line to both plots are so similar as to be almost indistinguishable. Although there are slight differences that will become more apparent in the next section when the luminosity function is discussed, it is clear that the objection raised by de Vaucouleurs that the shape of the upper envelope is crucially affected by a perturbation in the velocity field is not correct.

The same conclusion is reached from all the other (v_H, M_B^0)-diagrams plotted for each of the remaining bins (see Table 1). A few representative examples are given in Figures 2–4.

In Figures 2 and 3 the unperturbed model (zero infall) is panel *a*, and the 440 km s^{-1} infall case is panel *b*. No plots of the intermediate case of 220 km s^{-1} infall are shown as they are always bracketed by the two extreme models. Figure 2 shows all the spiral classes of all luminosity classes lumped together. Here the sample size is largest, but the range of Hubble types and vdB luminosity classes is also largest; nevertheless, the spread in absolute luminosities above the m_B limit line is only slightly larger than in Figure 1. Note also that the spread is slightly reduced in Figure 3, which shows only Sa and Sab galaxies.

Finally, in Figure 4 we show representative plots of the Sbc to Sc section of the Hubble sequence broken into four progressively fainter luminosity classes. Figure 4*a* shows the plots for the unperturbed (i.e., the ideal Hubble flow) model; Figure 4*b* for the 440 km s^{-1} infall case. Both are similar to Figure 1 of TYS, which shows the large overlap in absolute magnitude between different luminosity classes within a given Hubble type. Comparison of panels *a* and *b* here shows that *this overlap cannot be reduced by appeal to the properties of any reasonable model of the velocity perturbation.* Kennicutt also states that the overlap *remains* in his analysis as well.

In closing this section we note that the *centroid* of the absolute magnitude distribution does indeed move fainter in these diagrams as the luminosity class becomes later, ranging from $\langle M_B^0 \rangle \approx -21.5$ for luminosity class I–I.7 to $\langle M_B^0 \rangle \approx -20.0$ for class II.8–III in Figure 4*a* (a little fainter in Fig. 4*b*), in much the way given by van den Bergh (1982, his Table III), but it must be kept in mind that this procedure does *not* calibrate the absolute magnitudes of the luminosity classes, but merely gives $\langle M_B^0 \rangle$ for the *highly* biased sample of the RSA, which is severely apparent magnitude limited. We see only the tip of the iceberg of the true M_B^0 distribution in the (v_H, M_B^0)-plots. Samples to fainter *apparent* magnitude limits would extend the distributions to fainter absolute magnitudes, as evidenced by the fact that in Figures 1–4 each distribution abuts the lower limit line at $m_B \approx 13.2$. It must be strongly emphasized that the dispersions listed by van den Bergh in his cited table are the *apparent* dispersions of the *observed* distributions in diagrams such as Figures 1–4 and have nothing to say about the dispersion of the true luminosity functions, a problem discussed in the first two papers of the STY, YTS series, and also implicit in the discussion of the luminosity functions in the next section. The true functions are even broader than implied by the apparent dispersions.

III. THE EFFECT OF VELOCITY PERTURBATIONS ON CALCULATED LUMINOSITY FUNCTIONS

We now approach Kennicutt's suggestion that the true luminosity function of galaxies of a given luminosity class is

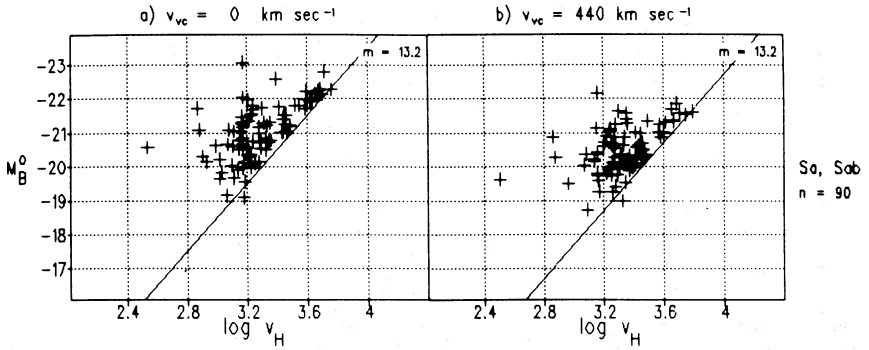

FIG. 3.—(*a*) Same as Figs. 1*a* and 2*a* for Hubble types Sa and Sab. (*b*) Same as Fig. 3*a* for the $v_{Vc} = 440$ km s^{-1} infall model.

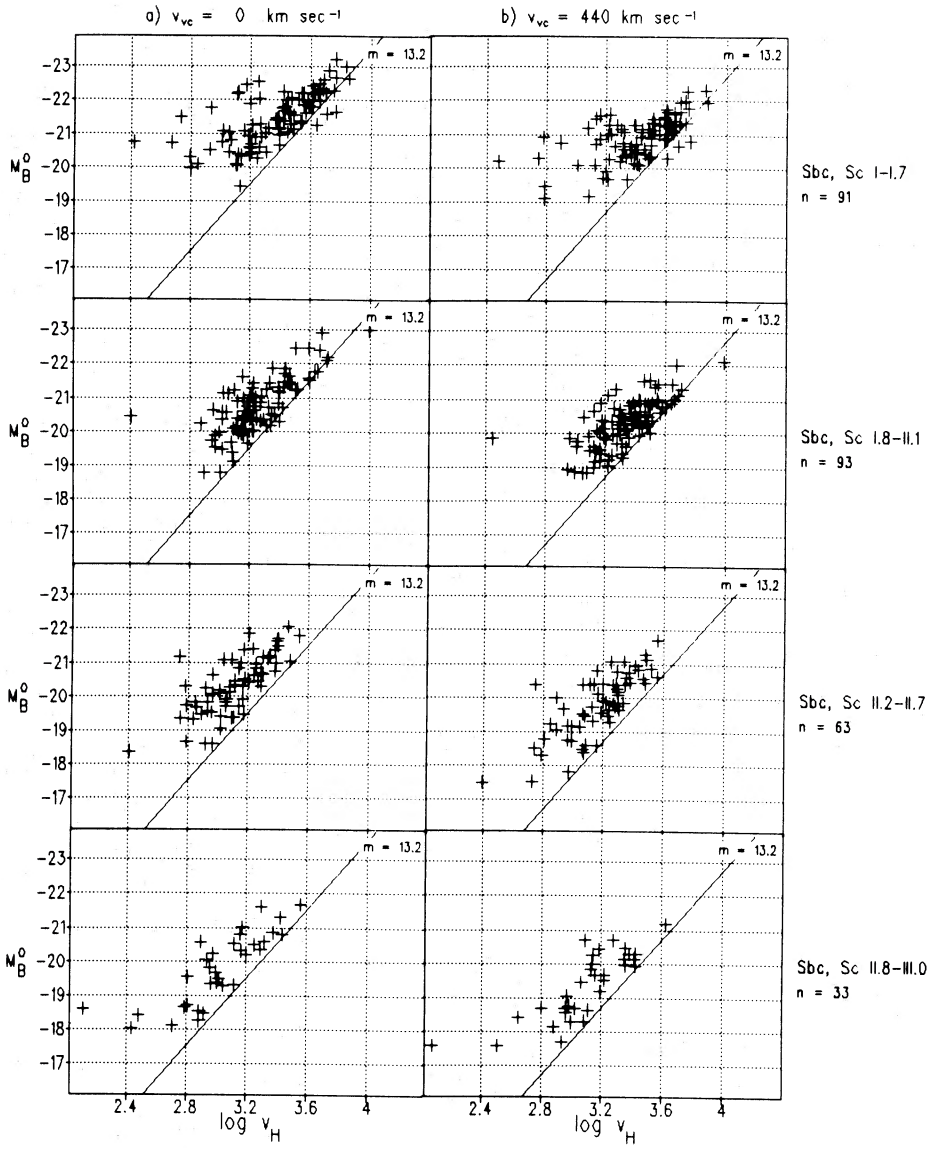

FIG. 4.—The (v_H, M_B^0)-diagram for Sbc plus Sc galaxies for four different luminosity class intervals: (*a*) for the zero infall model and (*b*) for the v_{vc} = 440 km s^{-1} infall model. Compare this diagram with Fig. 1 of TYS.

narrower than calculated by TYS. If true, especially for ScI galaxies, then one of the first attempts to extend the distance scale to redshifts $\gtrsim$ 10,000 km s^{-1} made by Sandage and Tammann in their Papers IV, V, and VI (1974, 1975*a*, *b*) would have found a modern justification. However, for reasons mentioned earlier his result was unexpected, leading to the present recalculation.

We have determined the luminosity functions for the 18 groups of Table 1 for all three infall models. The method can be understood from the discussion in § II*b* and the inspection of the (v_H, M_B^0)-diagrams: within each vertical strip with the width $\Delta \log v_H = 0.2$ a segment of the luminosity function is obtained which can be tacked onto the next more distant strip by multiplication with the volume ratio, in this case 3.98 = dex 0.6. Analogously, this procedure is realized differentially by assigning a weight to each galaxy according to the volume it is found in. A specific galaxy naturally will get a different volume weight $w(V)$ in each infall model.

However, the procedure is not yet correct in this simple form because the RSA is not a complete catalog to its stated magnitude limit of $B \approx 13.2$ but becomes progressively more incomplete as this limit is approached. We have applied corrections to the counted numbers of galaxies by multiplying each galaxy of apparent magnitude m with its proper weight $w(m) = f(m)^{-1}$, where $f(m)$ describes the completeness function of the RSA. The function $f(m)$ is known in explicit form (STY, Fig. 6). A galaxy with m = 12.0 mag, i.e., a magnitude where the RSA is essentially complete such that $f(12.0) = 1$, obtains the weight 1; a galaxy with m = 13.2 mag, however, carries the weight 11.1 because $f(13.2) = 0.09$. All RSA galaxies fainter than 13.2 mag were given zero weight.

This incompleteness factor on the apparent magnitudes of RSA galaxies affects most of the luminosity functions. It results, for instance, for SII and fainter galaxies, as well as for early-type galaxies, in an enhancement of the faint end of $\varphi(M)$, whereas for Sa, Sab galaxies the bright end is enhanced. Kennicutt did not apply this correction.

The luminosity functions were calculated with magnitudes

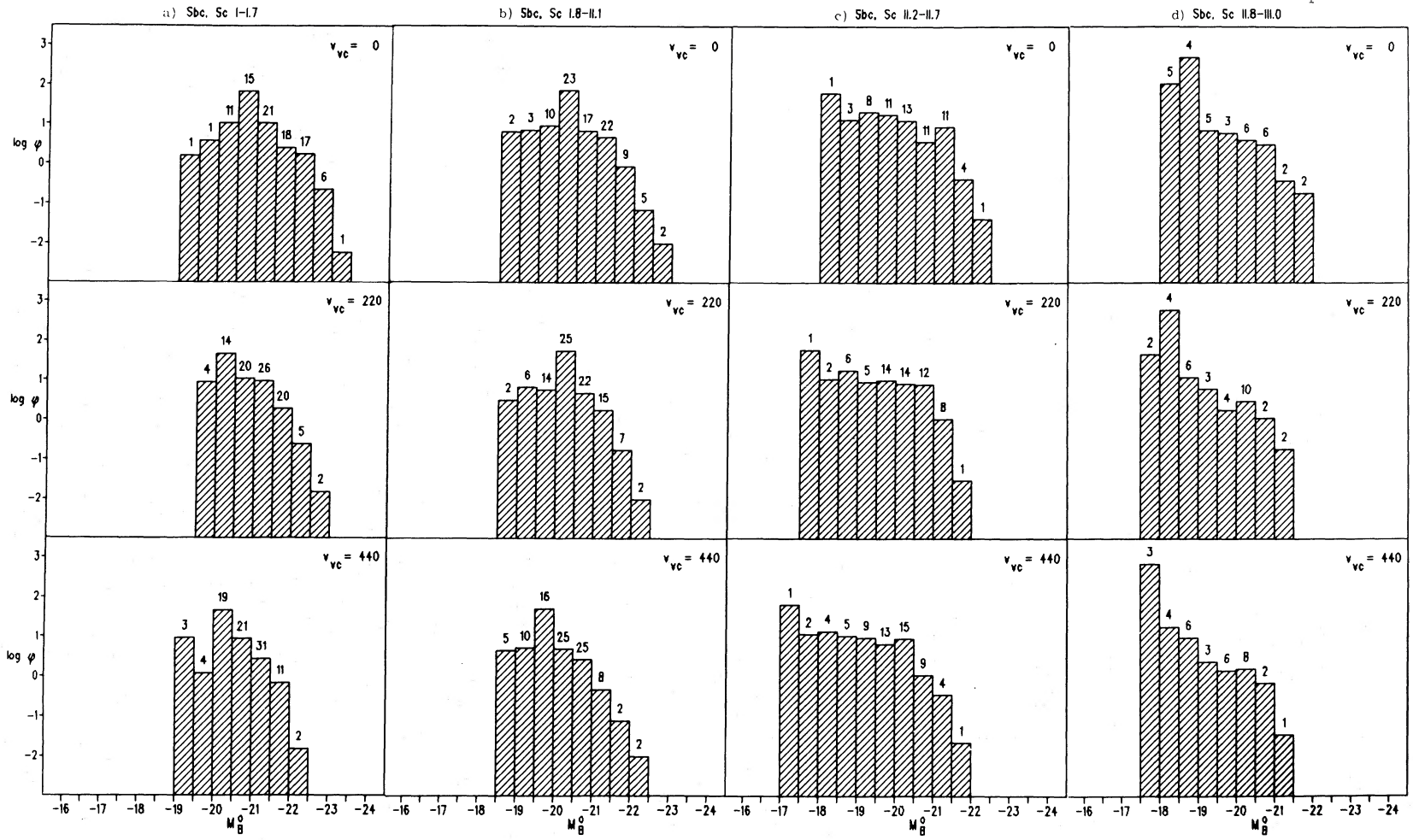

FIG. 5.—(*a*)–(*d*) The differential luminosity function for Sbc, Sc galaxies for the three infall models. The number of galaxies involved in the sums are marked. Because the distance to the Virgo Cluster is kept constant, the effective Hubble constants differ between the three panels, causing an artificial shift toward fainter magnitudes as the infall velocity increases. The zero point of the density scale, log φ, is arbitrary.

corrected for galactic absorption but not for internal absorption. Corrections for internal absorption demand stronger incompleteness functions, and because the Hubble type partly determines the amount of the correction, the incompleteness functions would become bin-dependent as well.

An inspection of the mean internal absorption $\langle A^i \rangle$ per magnitude interval does not produce a systematic increase or decrease with absolute magnitude for any of the 15 concerned bins. The luminosity functions based on magnitudes corrected only for galactic absorption, M_B^0, can therefore be transformed into luminosity functions based on magnitudes corrected for internal absorption too, $M_B^{0,i}$, through a shift of the mean internal absorption correction $\langle A^i \rangle$ of the considered subsample.

A representative set of differential luminosity functions is shown in Figures 5*a*–5*d* for Sbc, Sc spirals with a range of luminosity class of I-III. The Kennicutt falloff effect at faint magnitudes is not seen. Consider Figure 5*a*, for luminosity class I–I.7. For the $v_{Vc} = 0$ km s^{-1} model, $\varphi(M_B^0)$ appears to decrease fainter than $M_B^0 = -20.5$, albeit the numbers in the faintest three bins are very small. This decrease at the faint end agrees with the earlier result of TYS (their Fig. 3) for the spirals of type I to I–II. Note in Figure 5*a* that the decrease is not as obvious for the $v_{Vc} = 440$ km s^{-1} case.

The same conclusion follows from Figure 5*b*, for the luminosity class I.8–II.1. A maximum is reached that is half a magnitude fainter than for the luminosity class I–I.7, but the dispersion is very broad for all three models.

The magnitude range from $v_{Vc} = 0$ km s^{-1} to either $v_{Vc} = 220$ or 440 km s^{-1} tightens in Figures 5*a* and 5*b*, but the sharpness of $\varphi(M_B^0)$ never improves as drastically as was expected from Kennicutt's paper. Only 0.5–1 mag is gained.

Inspection of Figures 5*c* and 5*d* shows no improvement of the luminosity function at all from $v_{Vc} = 0$ to 440 km s^{-1}. The conclusion of TYS in their Figure 3 that no maximum in $\varphi(M_B^0)$ is reached to the limit of our data at $M_B^0 = -18$ for luminosity classes later than II is confirmed.[2]

In all these diagrams there is a shift in the absolute magnitudes between the three models. This is, however, artificial, due entirely to the change in the effective Hubble constant for the reason explained in § II.

Figures 6 and 7 show the similar situation for Hubble types E + E/S0 and S0 + S0/E. Two features of Figures 6 and 7 are noteworthy. (1) There is a strong difference in $\varphi(M_B^0)$ between E and S0 galaxies. There are many more faint S0's than faint E's

[2] We do not mean to imply by these results that there *is* no maximum to $\varphi(M)$ for spirals, but only (1) that this maximum is not yet reached at $M_B \approx -18.5$, and (2) that this conclusion is independent of any realistic Virgo perturbation strength. We know, in fact, from data on a complete sample of spirals in the Virgo core itself that no spirals exist there fainter than $B = 16.7$ ($M_B = -15$), and that $\varphi(M)$ does have a very broad maximum centered at $M_B = -18$, fully consistent with the results in Fig. 5.

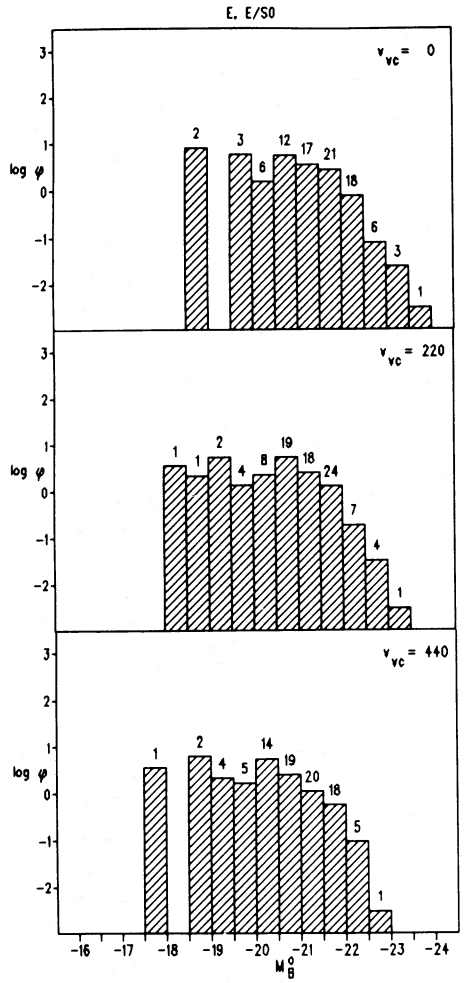

FIG. 6.—Same as Fig. 5 for E plus E/S0 types

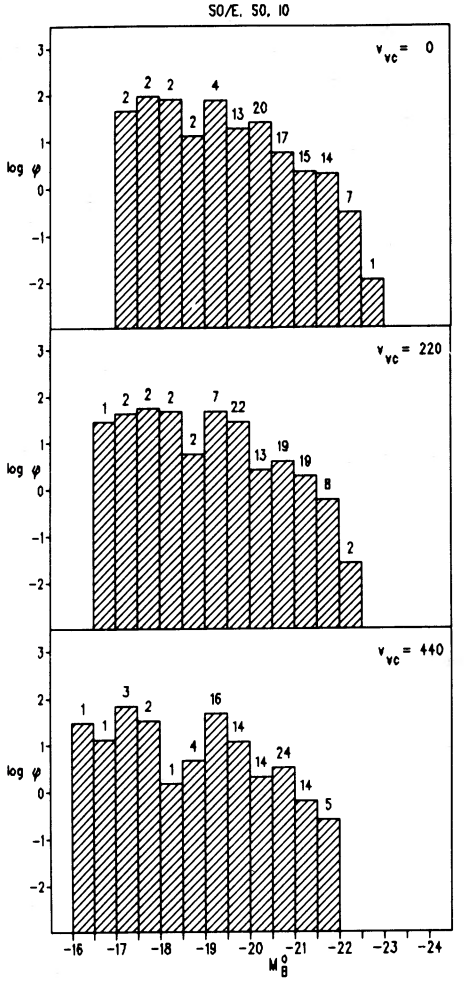

FIG. 7.—Same as Fig. 6 for S0 plus S0/E types

in the RSA sample, and the brightest E galaxies are brighter than the brightest S0's by about a magnitude. The same result was found previously in the Virgo Cluster sample itself (Kraan-Korteweg 1981), and by TYS in their analysis of the $v_{Vc} = 0$ km s^{-1} calculation of the RSA sample. (2) A gap may exist in the S0 $\varphi(M_B^0)$ near $M_B^0 = -18.5$, appearing in all three models, but the numbers are small.

IV. SUMMARY AND CONSEQUENCES

Absolute magnitudes and the luminosity functions therefrom have been computed for all RSA galaxies from their redshifts using three self-consistent velocity perturbation models characterized by assumed local Virgo infall velocities of $v_{Vc} =$ 0, 220, and 440 km s^{-1}. The results for different subsets of RSA galaxies, shown in the (v_H, M_B^0)-diagram, are insensitive to the value of v_{Vc}, contrary to an earlier suggestion by de Vaucouleurs (1983).

The luminosity function of spirals of a given van den Bergh luminosity class remains broad in all three infall models. Only $\varphi(M_B^0)$ for ScI–ScII galaxies turns over for magnitudes fainter than $M_B^0 \approx -19$, but even for them $\varphi(M_B^0)$ is broad. All luminosity functions of later luminosity classes continue to rise to the limit of our data on the faint end at $M_B^0 \approx -18$. The result weakens earlier hopes that luminosity classes are reliable distance indicators (van den Bergh 1960; Paper IV; Kennicutt 1982). The broadness of the individual $\varphi(M)$ functions in the narrowly restricted bins of Hubble type *and* luminosity class also shows that de Vaucouleurs's "luminosity index" Λ has a wide dispersion, which is sometimes artificially masked by a bright catalog limit in apparent magnitude. The broadness of the individual luminosity functions means that the mean M_B-value of Λ even for a narrowly restricted galaxy type becomes fainter as the apparent magnitude limit of any given sample is made fainter, which is, of course, the Malmquist bias. The effect is seen directly in the behavior of Λ for Virgo Cluster spirals as one samples deeper and deeper into the cluster luminosity function (Tammann and Sandage 1982).

The purpose of the present paper is to show that these conclusions do not depend on the velocity perturbations of the RSA sample for any reasonable values of v_{Vc} and hence are independent of the Virgo complex perturbation.

REFERENCES

Branch, D., Falk, S. W., McCall, M. L., Rybski, P., Uomoto, A. K., and Wills, B. J. 1981, *Ap. J.*, **244**, 780.
Davis, M., Geller, M. J., and Huchra, J. 1978, *Ap. J.*, **221**, 1.
de Vaucouleurs, G. 1979, *Ap. J.*, **227**, 380.
———. 1983, *M.N.R.A.S.*, **202**, 367.
de Vaucouleurs, G., de Vaucouleurs, A., and Corwin, H. G. 1976, *Second Reference Catalog of Bright Galaxies* (Austin: University of Texas Press) (RC2).
Dressler, A. 1984, *Ap. J.*, **281**, 512.
Geller, M. J., and Davis, M. 1978, *Ap. J.*, **225**, 1.
Kennicutt, R. C., Jr. 1982, *Ap. J.*, **259**, 530.
Kraan-Korteweg, R. C. 1981, *Astr. Ap.*, **104**, 280.
———. 1984, in preparation.
Panagia, N., *et al.* 1980, *M.N.R.A.S.*, **192**, 816.
Peebles, P. J. E. 1976, *Ap. J.*, **205**, 318.
Sandage, A. 1972, *Ap. J.*, **178**, 25.
———. 1982, private communication.
Sandage, A., and Tammann, G. A. 1974, *Ap. J.*, **194**, 559 (Paper IV).
———. 1975*a*, *Ap. J.*, **196**, 313 (Paper V).
Sandage, A., 1975*b*, *Ap. J.*, **197**, 265 (Paper VI).
———. 1981, *A Revised Shapley-Ames Catalog of Bright Galaxies* (Washington, D.C.: Carnegie Institution of Washington) (RSA).
———. 1982, *Ap. J.*, **256**, 339 (Paper VIII).
———. 1983*a*, in *Astrophysical Cosmology: Proceedings of the Study Week on Cosmology and Fundamental Physics*, ed. H. A. Brück, G. V. Coyne, and M. S. Longair (Vatican City: Pontificia Academia Scientiarum), p. 23.
———. 1983*b*, *Nature*, **307**, 326.
———. 1984, *Ap. J.*, in preparation.
Sandage, A., Tammann, G. A., and Yahil, A. 1979, *Ap. J.*, **232**, 352 (STY).
Schechter, P. L. 1980, *A.J.*, **85**, 801.
Silk, J. 1974, *Ap. J.*, **193**, 525.
Tammann, G. A., and Sandage, A. 1982, *Highlights of Astronomy*, **6**, 301.
Tammann, G. A., Yahil, A., and Sandage, A. 1979, *Ap. J.*, **234**, 775 (TYS).
Tonry, J. L. 1980, Ph.D. thesis, Harvard University.
Tonry, J. L., and Davis, M. 1981, *Ap. J.*, **246**, 680.
van den Bergh, S. 1960, *Ap. J.*, **131**, 215.
———. 1982, *Pub. A.S.P.*, **94**, 745.
Yahil, A., Tammann, G. A., and Sandage, A. 1980, *Ap. J.*, **242**, 448 (YTS).

RENÉE C. KRAAN-KORTEWEG and GUSTAV A. TAMMANN: Astronomisches Institut der Universität Basel, Venusstr. 7, CH-4102 Binningen, Switzerland

ALLAN SANDAGE: Mount Wilson and Las Campanas Observatories, 813 Santa Barbara Street, Pasadena, CA 91101